Spatial-mode dynamics in a photorefractive ring oscillator with induced astigmatism

S. Juul Jensen

Optics and Fluid Dynamics Department, Risø National Laboratory, P.O. Box 49, DK-4000 Roskilde, Denmark

R. Nicolaus and C. Denz*

Institut for Applied Physics, Darmstadt University of Technology, Hochschulstr. 6, D-64289 Darmstadt, Germany

We report experimental observations of the mode dynamics in a weakly multimode photorefractive ring oscillator with induced astigmatism. First a gallery of transverse, higher-order Gaussian modes in the system is presented. Subsequently the dynamics of beating modes and the interactions between modes belonging to different bases are examined. The latter show the transition of modes between the three equivalent mode families experimentally. Finally regions of cavity symmetry leading to different spatial modes and mode dynamics are identified. © 2001 Optical Society of America

OCIS codes: 190.5330, 140.4780, 030.4070, 190.4420.

1. INTRODUCTION

The transverse spatial structure of the light field in a nonlinear optical oscillating system reveals a fascinating world beyond the fundamental Gaussian mode. When the intracavity aperture is increased, a number of spatiotemporal structures appear above a certain threshold. The degree of freedom in such a resonant system is characterized by the cavity Fresnel number F, relating the diffraction of the fundamental Gaussian to the geometrical angle set by the elements of the system. For small openings, leading to a low degree of freedom, the field is quite accurately described by the modes of an empty optical cavity. When the degree of freedom is further increased, a global description of the field is appropriate with phenomenological amplitude equations similar to the ones used in hydrodynamics. Although the laser is the typical example used in investigations of the lower- and the higher-order regimes of transverse degrees of freedom, a photorefractive ring oscillator (PRO) (see e.g., Refs. 1–6) is much better suited for investigation of spatial-mode physics, especially when it comes to the study of spatiotemporal dynamics. The advantages of the PRO are due mainly to its inherently slow dynamics (≈ 1 Hz), making dynamic structures easy to observe and record with CCD cameras. Moreover, it exhibits a narrow gain linewidth (≈ 1 Hz), leading to a precise selection of structures, and a broad and continuous tuning range through several free spectral ranges, giving a complete set of structures in the system. Finally the requirement of only a few milliwatts of laser power to pump the cavity allows us to investigate these structures with standard laser devices.

In the weakly multimode case, where the Fresnel number F is low ($F < 5$), the PRO has been shown to contain both stationary and dynamic structures described by higher-order Gaussian modes.[6] These can theoretically be Hermite modes (modes that belong to a Cartesian symmetry), Laguerre modes (modes of a resonator with circular symmetry), or doughnut modes (circular symmetric modes with one or more phase dislocations in the center, occurring only in systems of perfect rotational symmetry). They are symmetric by a given rotation, in contrast to the Laguerre flower modes, which are rotationally symmetric at discrete angles governed by the mode order. Because focusing elements are often included in photorefractive resonators to enhance optical stability, Laguerre modes should be the prevailing solutions provided that the resonator is adjusted symmetrically to the optical axis.

Higher-order modes are ordered into families of near frequency degeneracy. The frequency regions of the different mode families and the dynamics between modes overlapping in frequency space have been explored in the unidirectional PRO.[3] Dynamic patterns can be observed between modes both of the same family and of different families.[6] The temporal repetition of the mode order in a PRO when the cavity length is tuned by natural drift, i.e., left alone, is seen to be periodic for low Fresnel numbers, but higher F-values may introduce chaotic itinerancy and even spatiotemporal chaos.[7]

In the PROs examined so far the attention has been on cylindrical symmetric systems, where astigmatism and misalignment have not been considered. However, this situation does not correspond to realistic experimental configurations, where often the natural cylindrical symmetry is broken by nonperfect components, imperfect alignment, or by intentionally induced directional losses such as Brewster windows. This induces an astigmatism in the system, leading to a certain frequency separation of perpendicular modes belonging to the same mode family, i.e., the frequency degeneration is broken. Because of the nonlinearity inside the cavity, the losses in one direction are often stronger than in the other, and the system will prefer this direction for oscillation. In one of the lat-

est contributions to this subject a PRO with induced astigmatism was investigated for the one-dimensional case.[8] In the two-dimensional case, Hermite modes are the higher-order modes most often observed, even though Laguerre modes can still be obtained. Therefore much richer mode dynamics can be expected in a realistic two-dimensional PRO, because the structures belonging to two different mode bases can be apparent in the system at the same time. This takes place either going from a rectangular to a cylindrical symmetry or from a cylindrical to a full rotational symmetry. Which mode description is adequate depends on the transverse symmetry of the system. The different mode bases are fully equivalent and can be transformed into each other by a proper choice of phase shifts and amplitude relations between the modes.

We investigate a system in which modes of different bases interact, showing the equivalence between the mode descriptions experimentally. Although the transformation from modes of one family into the modes of another by superposition is mathematically well known, it has been unclear how the corresponding spatiotemporal dynamics of modes is affected by this mode competition. Therefore we investigate schemes of mode transition for different values of induced astigmatism that leads to different degrees of symmetry. We also identify the symmetry regions leading to the dynamics between the mode structures, and finally to phase locking between the modes.

2. EXPERIMENTAL CONFIGURATION

Our unidirectional PRO consists of four mirrors with an intracavity lens ($f = 300$ mm) and a perimeter of 790 mm, as shown in Fig. 1. It is pumped by two-beam coupling in a nominally undoped $BaTiO_3$ crystal of the size $a \times b \times c = 3.15$ mm $\times$ 2.35 mm $\times$ 6.25 mm.

A frequency-doubled Nd:YAG laser at wavelength 532 nm is used to pump the resonator, yielding a pump-beam diameter of approximately 2 mm inside the crystal. Pump powers between 20 and 30 mW are used in these experiments. The external angle between the pump beam and the resonator beam is approximately 30°, and between the pump beam and the crystal c axis, approxi-
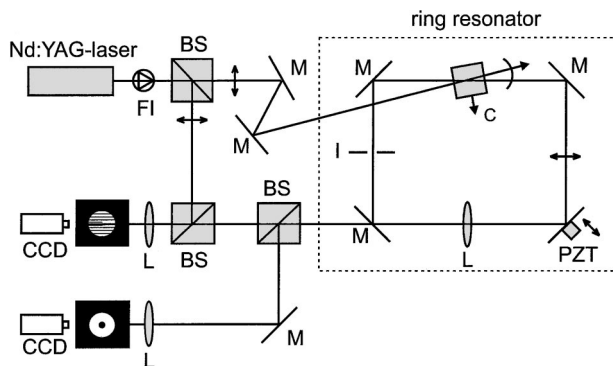

Fig. 1. Experimental configuration of the unidirectional PRO with induced asymmetry. FI, Faraday rotator; BSs, are beam splitters, Ms, mirrors; Ls, lenses, I, iris aperture, PZT, is a piezo-driven mirror; CCDs, CCD cameras; C optical c axis of the $BaTiO_3$ crystal. The arrows indicate the beam polarization and translation of PZT.
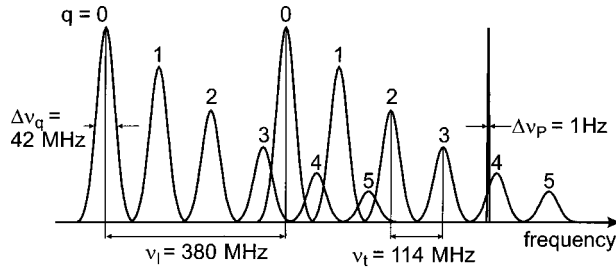
mately 85°. This orientation aligns the wave vector of the two-beam coupling grating relative to the c axis, and exploits the large electro-optic r_{42} coefficient of the $BaTiO_3$ crystal. Considerations of the cavity geometry lead to a resonator-beam diameter inside the crystal of approximately 1.35 mm. A two-beam coupling gain of $V = I_{S1}/I_{S0} \propto \exp(2\Gamma_l)$ is measured[9] with $\Gamma_l = 3$, 5 $\pm$ 0, 5.

The resonator is aligned with a reference beam injected along the expected path of the resonator beam but circumventing the crystal on a small additional path, not shown in Fig. 1. This beam is exploited to actively stabilize the resonator by using a lock-in amplifier technique.[6] When the pump beam is switched on, a resonator beam with a transverse-mode structure easily arises owing to scattered light inside the crystal propagating along the optical axis.

One of the mirrors is mounted on a piezoelectric transducer to vary the cavity length. The transverse degree of freedom is limited by an iris varying the cavity Fresnel number between 2 and 15. These values correspond to an aperture diameter of 1 mm and an open aperture where the transverse degree is limited by the finite size of the pump beam, respectively. Typically the iris is adjusted to suppress modes of orders higher than 4, which roughly corresponds to the Fresnel number. The reflectivity equivalent, R_{eq}, of the resonator is approximately 0.5 as a result of the uncoated crystal inside.

Our primary parameters to control the resonator symmetry are the transverse position of the intracavity lens and the transverse position of the iris. The angle between the crystal and the pump beam or the grating vector can be varied by approximately $\pm 10°$, and oscillation can still occur. This is because of a coupling strength well above threshold. A change of the angle is seen to affect the transverse symmetry only slightly. The modes are extracted from the cavity by one of the mirrors, divided into two beams by a beam splitter, and magnified onto two CCD cameras by lenses of short focal length. To image phase dislocations, one of the beams is made to interfere with a plane reference beam.

The longitudinal mode separation, i.e., the free spectral range, of the resonator is $\nu_l = c/L = 380$ MHz, where $L = 790$ mm is the perimeter of the resonator and c is the free-space speed of light. Higher-order transverse modes require an additional phase shift to fulfill the resonance condition of a cavity containing focusing elements. The transverse mode separation, ν_t, for the ring resonator is given by[10]

$$\nu_t = \left[\frac{1}{2\pi} \arccos\left(1 - \frac{L}{2f} \right) \right] \frac{c}{L} = 114 \text{ MHz}, \qquad (1)$$

where $f = 300$ mm is the focal length of the lens. Therefore the resonator contains 3.32 transverse mode spacings per free spectral range; hence, the fundamental mode is placed between the third- and the fourth-order mode. This is consistent with our experimental observations. Because of a continuous change of the resonator length realized by the movable mirror in the cavity, we observed the mode sequence presented in Fig. 2.

Fig. 2. Transverse mode arrangement of the PRO. ν_l and ν_T are the longitudinal and transverse mode spacing, $\Delta\nu_q$ is the width of a transverse mode, q is the mode family number, and $\Delta\nu_P$ is the narrow linewidth of the two-beam coupling gain.

The FWHM, $\Delta\nu_m$, of a single mode is determined by the reflectivity equivalent of the cavity, $R_{eq} = 0.5$, and is given by[11]

$$\Delta\nu_m = \nu_1\left[\frac{1 - (R_{eq})^{1/2}}{\pi(R_{eq})^{1/4}}\right] = 42\,\text{MHz}. \qquad (2)$$

Because of the intracavity iris, the transverse modes experience diffraction loss that increases with mode order. This broadens the linewidth for the higher-order modes, and thus the value of $\Delta\nu_m$ given in Eq. (2) should be taken as a minimum. The transverse-mode arrangement shown in Fig. 2 indicates that there are frequency regions where the gain curves of different mode families overlap, allowing modes of two different families to become excited simultaneously. Figure 2 also shows the gain linewidth of the pump beam, $\Delta\nu_{\text{pump}}$, of the PRO that is of the order of a few hertz, which is determined by the narrow-band two-beam coupling gain of the photorefractive crystal. This is quite different from a typical gas laser, where the gain linewidth is of the order of gigahertz, covering several free spectral ranges. In those lasers, in principle, all mode families could be excited at the same time, neglecting diffraction losses and spatial holeburning effects. Typically, mode competition limits the oscillation to a few modes only. However, observing the dynamic behavior between different modes in lasers requires internal apertures to choose between the transverse modes. Mode beatings are typically of the order of hundreds of kilohertz and thus are difficult to resolve by commercial equipment.[12] In contrast, in the case of the PRO, strong frequency pulling results in mode dynamics of the order of 1 Hz or less,[3] a time scale that is easily accessible by standard registration devices. Moreover the gain curve of a laser is much broader than the mode resonances, as opposed to the PRO, where the gain curve is below 1 Hz, owing to the narrow Bragg condition. Therefore the desired spectral position can be adjusted accurately.

In our experiments we tune the cavity length through a full free-spectral range and video record the structures and the dynamics of the different families at stationary lengths. This is done for an increasing degree of cavity symmetry, mainly adjusted by the transverse position and tilt of the intracavity lens. With our active cavity stabilization, regions of mode beating can be easily adjusted. The recorded sequences of mode transition then appear spontaneously without any further intervention.

3. TRANSVERSE MODES AND MODE DYNAMICS

The modes of the weakly multimode PRO are quite accurately described by the empty-cavity modes of a typical laser cavity, even though this description is only an approximation that is valid in the case of infinitely large apertures. Modes can be projected onto three different bases, depending on the dominant system geometry, which are the Gauss–Hermite, the Gauss–Laguerre, and the Gauss–doughnut modes. In theory, all modes of the same higher-order mode family are frequency degenerate, and the three mode bases are fully equivalent. However, depending on the cavity symmetry, the frequency degeneracy of the higher-order modes is broken, leading to modes belonging mainly to one description.

A. Higher-Order Transverse Modes
When tuning the resonator length, it is possible to obtain almost every transverse mode of the different bases, adjusting the resonator symmetry by the lens tilt.

At first we adjust Hermite modes for a rectangular-symmetry setting. As shown in Fig. 3, most transverse modes up to the fourth family are obtained. Only the H_{40} and H_{04} modes are missing. This could be because the lateral sizes of these modes are larger than the others. Therefore the aperture opening probably is too narrow, and the modes are simply blocked.

Then the lens is adjusted to a cylindrical symmetry, and thus circular modes arise as shown in Fig. 4. Laguerre modes up to the fourth family are obtained except for A_{032}, A_{042}, A_{121}, and A_{20}. The missing modes indicate that the cylindrical symmetry is broken in a radial distance affecting only modes of orders higher than 2.

Not all of the modes shown are stable in this particular arrangement, because orthogonal modes are close in frequency and thus beat with each other. Modes in one direction can be stabilized by inducing losses for the orthogonal mode by inserting an appropriate aperture or obstruction; e.g., a hair, which will break the full rota-
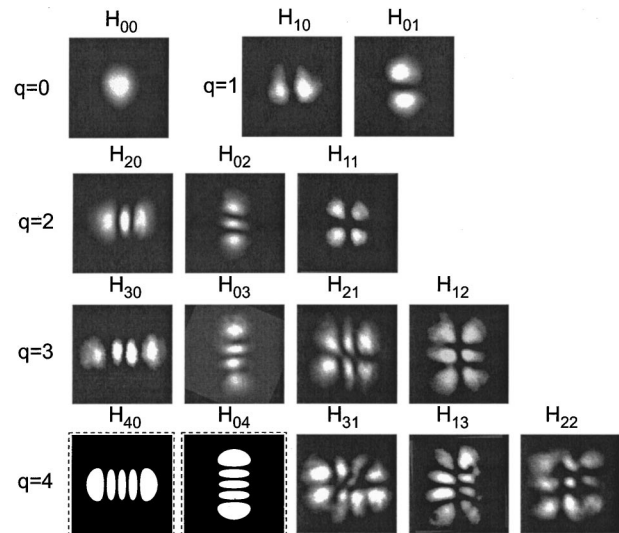

Fig. 3. Experimental intensity patterns of transverse Hermite modes. Mode families up to the order of $q = 4$ are shown. The modes in the dashed boxes are theoretical plots.
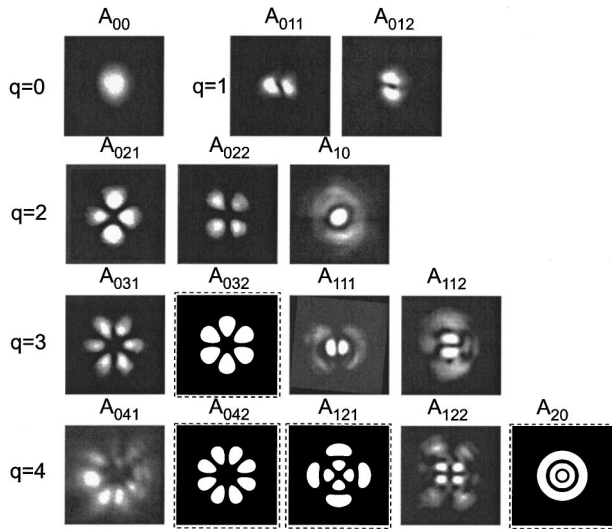
Fig. 4. Experimental intensity patterns of transverse Laguerre modes. Mode families up to the order of $q = 4$ are shown. The modes in the dashed boxes are theoretical plots.
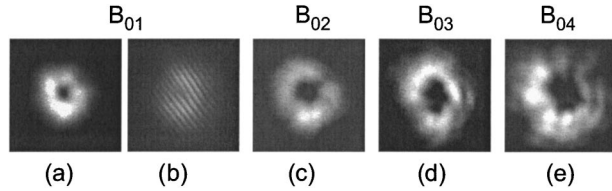

Fig. 5. Experimental intensity patterns of transverse doughnut modes. (a) First-order doughnut mode, (b) phase dislocation in the center of the mode, (c)–(e) second-, third-, and fourth-order doughnut mode, respectively.

tional symmetry.[13] When two orthogonal flower modes are close in frequency, they ideally lock into a stable doughnut mode [see Fig. 5(a)], proving that full rotational symmetry is obtained up to the second-order family. The interferogram of Fig. 5(b) shows a phase dislocation, or a vortex, in the center of the first doughnut mode. Doughnut modes of orders 2, 3, and 4, shown in Figs. 5(c)–5(e) are obtained as transient patterns existing 2–4 in dynamic mode-beating sequences. The number of phase dislocations in the center of the doughnut corresponds to the number of the mode order. This is visible in Figs. 5(c)–5(e) as the dark center of the doughnuts increases with the mode order.

B. Beating between Higher-Order Modes

The PRO shows a vivid range of mode dynamics due to beatings between different transverse modes present under the gain curve at the same time. The mode beatings can be divided into intra-family and inter-family interactions. Intra-family mode dynamics occur because of beatings between modes belonging to the same family. The inter-family beatings are between modes of different orders. The time of the dynamics depends on the frequency separation between the interacting modes. The frequency separation between two modes of the same family is caused by a broken rotational symmetry caused by astigmatism induced by imperfect intracavity elements or a misalignment. In contrast, the frequency separation between two beating modes of different fami-

lies depends on the transverse-mode spacing, which is set by the cavity configuration. However because of the extremely narrow gain line of the photorefractive pump beam, $\Delta \nu_p \sim 1$ Hz, the transverse modes experience a high degree of frequency pulling. The dynamics is governed by the frequency separation of the frequency-pulled modes and not by their actual separation determined by the cavity.

A first order approximation gives the pulled frequency of an oscillating mode, ν_{osc}, as the weighted average between the pump-beam frequency, ν_p, and the frequency of the cavity mode, ν_m, expressed as[14]

$$\nu_{osc} = \left. \frac{\dfrac{\nu_p}{\Delta \nu_p} + \dfrac{\nu_m}{\Delta \nu_m}}{\dfrac{1}{\Delta \nu_p} + \dfrac{1}{\Delta \nu_m}} \right|_{> \nu_m \gg \Delta \nu_p}$$

$$= \nu_p + \nu_m \frac{\Delta \nu_p}{\Delta \nu_m}. \tag{3}$$

This expression shows that the oscillation frequency of a mode will be dominated by the narrowest linewidth, i.e., $\Delta \nu_p$. Because all the interacting modes will be strongly pulled toward the same pump frequency, ν_p, the dynamics between the oscillating modes will also be governed by the pump linewidth, $\Delta \nu_p$.

Throughout this section we emphasize modes that are rotated with respect to Cartesian coordinates, e.g., a rotated H_{02} mode becomes H'_{02}. This rotation is due to an inherent asymmetry in the cavity, and the marked H'_{02} and H'_{20} are obtained by superposition of H_{20} and H_{02} with appropriate phase shifts.

1. Intrafamily Mode Beatings

Owing to the induced astigmatism in the resonator, the frequency degeneracy of the family modes is broken. When the cavity length is stable, the modes begin to beat in a periodic sequence with a period depending on the frequency separation between the frequency-pulled modes. Periodic mode beatings in the second-order family are shown in Fig. 6. The figure shows two periodic sequences where the A'_{021} Laguerre mode beats with the A_{10} mode. Yet the sequences are of different time duration: the period of sequence I is 20 s compared with 42 s for sequence II. In fact, sequence I corresponds to the first 20 s of sequence II, i.e., approximately half the sequence. Starting from the twelve o'clock position, the A'_{021} Laguerre mode transforms into a linear H_{02} mode and further into the rotational symmetric A_{10} mode. In the following we use the expression "linear" for Cartesian modes when one index equals zero.

Then the ring of A_{10} separates into a superposition pattern referred to as $4H'$ (four holes).[15] This behavior is equal for the two sequences. In sequence I the $4H'$ pattern is oriented along the same axis as the A'_{021} mode that started the sequence, and it transforms into this, closing the periodic sequence. In contrast, the $4H'$ pattern of sequence II is rotated approximately 30° with respect to the
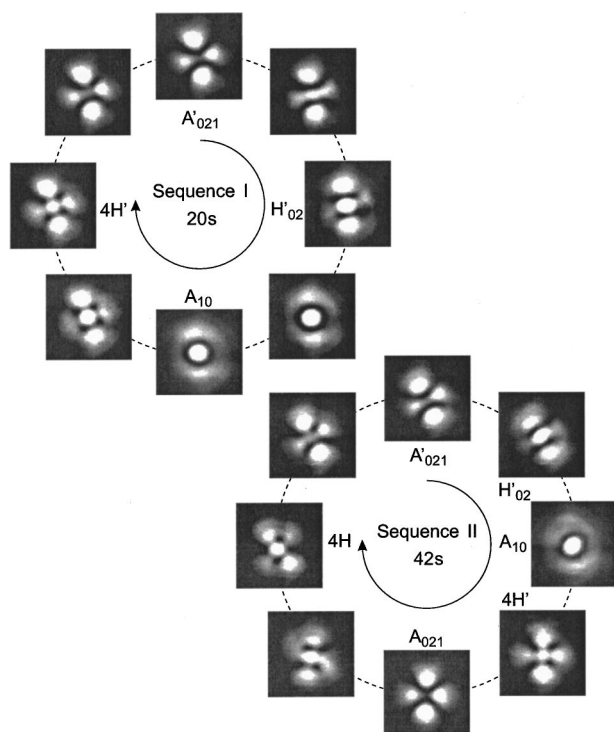
Fig. 6.   Two examples of periodic mode beatings in the second-order mode family.   I shows the sequence $A'_{021} \rightarrow H'_{021} \rightarrow A_{10}$ $\rightarrow 4H' \rightarrow A'_{021}$.   The first half of sequence II is almost equal to I, but ends at A_{021}, the second half of II shows an alternative rout from A_{021} to A'_{021}.

A'_{021} mode it originated from.   Therefore the $4H'$ pattern transforms into an A_{021} mode in another direction than it began for the sequence.   However, this A_{021} mode is perfectly shaped and oriented along the cavity axes, which suggests that it is a pure Laguerre mode indicating a higher symmetry than for sequence I.   This A_{021} mode then turns into the $4H$ pattern orthogonal to the first, and further into the starting A'_{021} mode closing the sequence.   Note that this transformation from A_{021} to A'_{021} takes as much time as a full sequence I.

This can be explained as follows: the A'_{021} mode is obtained as a superposition between the H'_{02} and the H'_{20} mode with a phase shift of π.   The beat period between H'_{02} and H'_{20} is approximately 20 s.   When the cavity is close to cylindrical symmetry, the linear modes become less dependent on direction.   This allows them to rotate. To obtain the A_{021} mode another pair of Hermite modes, H_{02} and H_{20}, still need a phase shift of π, which double to complete the period.   This indicates that the symmetry in sequence II is slightly increased with respect to sequence I.

Another kind of characteristic intrafamily dynamics is a nonperiodic transition from one mode to another. These transitions occur as very long transients when the system is on the border between two symmetries.   They can be associated with an unstable state of coexisting modes, giving rise to interesting dynamics where linear, circular, and doughnut modes interact.   In particular, it becomes possible to see how the linear modes superimpose to transform into the circular ones.   Starting with the first-order family, Fig. 7 shows how the doughnut

mode B_{01} is obtained as a superposition of the H'_{10} and the H'_{01} Hermite modes, or equivalently, by the A'_{011} and A'_{012} Laguerre modes.   The transition starts with a stable H'_{10} mode that becomes influenced by the orthogonal H'_{01} mode and together they superimpose to become a doughnut.   However their frequencies are too distant to frequency lock, and the doughnut splits in the opposite direction from which it formed to transform into the H'_{01} mode.   The H'_{01} mode is then stable or stays stable for a certain time and is then modified again by traversing another transient.

Figures 8 and 9 show transitions in the second order mode family.   In Fig. 8 a linear Hermite mode, H'_{02}, is transformed into the doughnut mode, B_{02}, and then into a linear mode in a near-perpendicular direction, H'_{20}. This transition is similar to the one shown in Fig. 7 for the first-order modes.   However, to obtain the B_{02} doughnut mode a superposition of all three second-order Her-
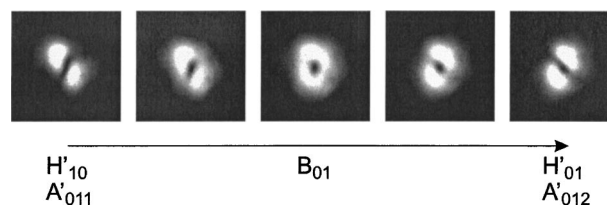

Fig. 7.   Mode transition in the first-order mode family.   The first-order doughnut mode B_{01} is obtained as a superposition of the Hermite mode H'_{10} and H'_{01} or the Laguerre modes A'_{011} and A'_{012}.
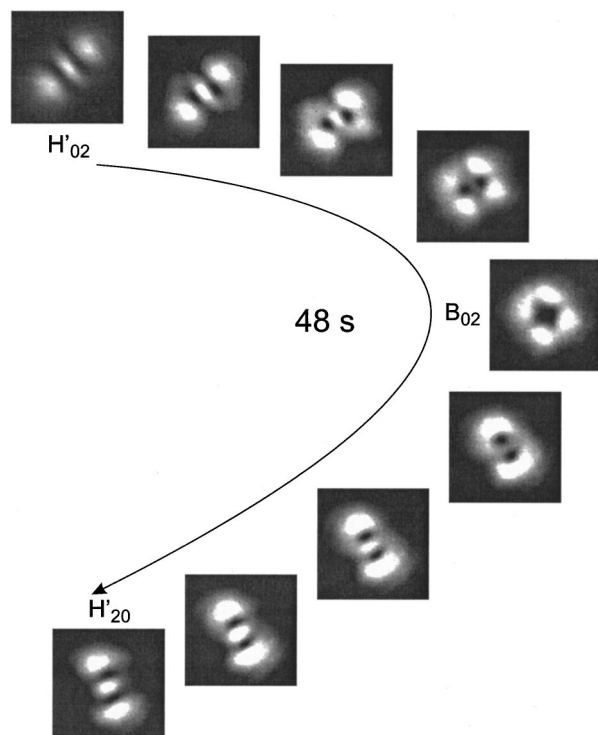

Fig. 8.   Example of a mode transition in the second-order mode family, from the H'_{02} to the H'_{20} Hermite mode.   The second-order doughnut mode B_{02} is obtained as a superposition of the modes H'_{02}, H'_{20}, and H'_{11}.   The H'_{11} mode can be identified in the picture just before the B_{02} mode.
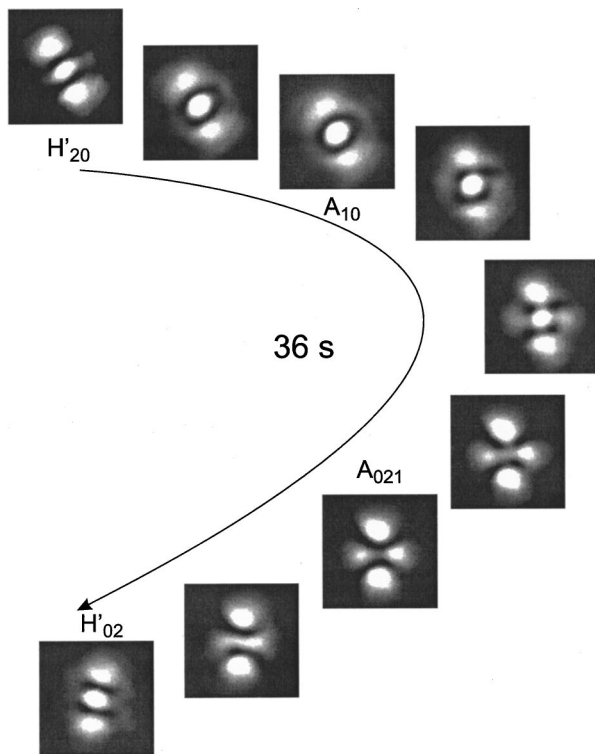
Fig. 9.   Another example of a mode transition in the second-order mode family, from the H'_{20} to the H'_{02} mode. The Laguerre modes A_{10} and A_{021} are obtained as superpositions of H'_{20} and H'_{02} with a phase shift of 0 and π, respectively.
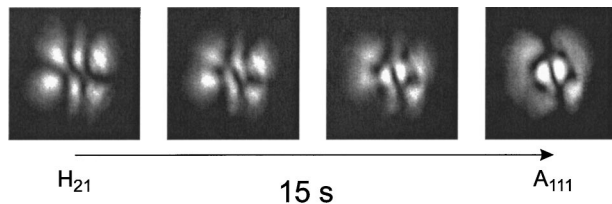

Fig. 10.   Example of a mode transition in the third-order mode family, passing from the H_{21} Hermite mode to the A_{111} Laguerre mode.

mite modes is necessary, i.e., $H_{20} + H_{02} + H_{11}$, with appropriate phase shifts. Indeed, the H_{11} mode participates in the transition, and it almost revealed itself in the picture before the doughnut mode. Figure 9 shows a transition from H'_{20} to H'_{02} passing through the A_{10} and A_{021} Laguerre modes. Theoretically A_{10} is a superposition of H_{20} and H_{02} with no phase shift, whereas the A_{021} mode requires a phase shift of π.

In both sequences it is possible to follow how the linear mode in one direction becomes more and more influenced by the mode in the near-perpendicular direction. The transformation from one mode to the other includes intermediate modes that theoretically can be obtained as superpositions of the linear modes. The equivalence between the different mode descriptions then becomes directly apparent. It should be noted that all these transitions are observed to occur in the same order several times, indicating a completely deterministic and reproducible behavior.

Figure 10 and Fig. 11 show examples of transitions in the third-order family. Figure 10 shows how the H_{21} Hermite mode transforms into the A_{111} Laguerre mode. The H_{21} mode contracts around its horizontal axis causing the four outer spots to melt together in pairs to form the two semicircles of the A_{111} mode. Simultaneously, the central spots drift by each other into a position rotated 90° from their initial orientation, forming the central part of the A_{111} mode. This happens because of the presence of the H_{12} mode, which superimposes with the H_{21} mode. Figure 11 shows a longer sequence where the linear H_{30} mode transforms into the A_{111} mode and further into the A_{031} flower mode. Finally, it turns into the linear H_{12} mode. This is a typical example of how the linear modes form different circular modes as they superimpose with different phase shifts.

From the mode transitions in Figs. 8 through 11, it becomes obvious how the theoretical equivalence between the different mode bases manifests itself experimentally. A mode from one basis is transformed into a mode from another basis by the presence of one or more other superimposing modes. The superimposing modes may or may not become visible during the transformation.

It should be noted that all of the dynamics between the interacting modes are in the range of 20–60 mHz, which is approximately an order of magnitude lower than the inverse photorefractive response time for this experiment. Furthermore the frequency of the dynamics decreases with increasing cavity symmetry. In contrast, the temporal dynamics of mode beatings in the experiments reported[3] are measured to be of the order of the photorefractive response time. This suggests that the temporal
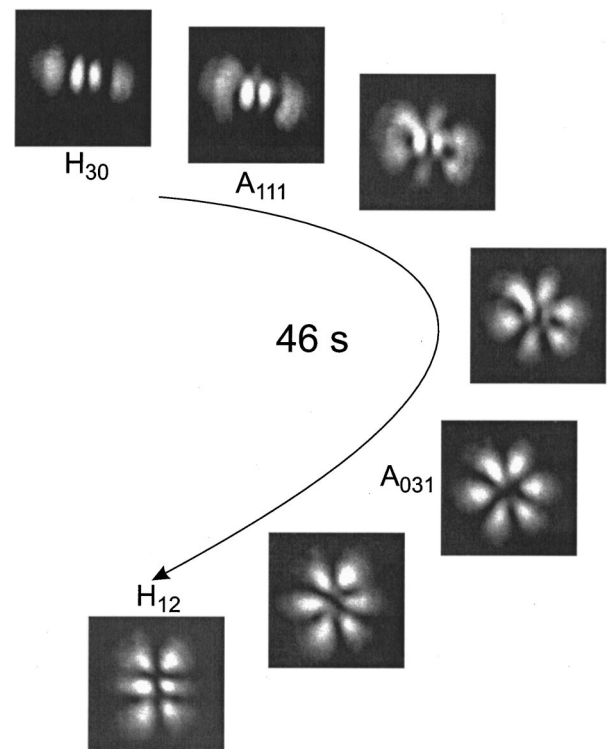

Fig. 11.   Another example of a mode transition in the third-order mode family, passing from the H_{30} to the H_{12} Hermite mode. The Laguerre modes A_{111} and A_{031} are obtained as superpositions of the H_{30} and H_{12} modes with appropriate phase shifts.
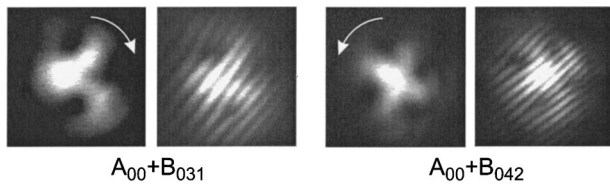
Fig. 12. Example of interfamily mode interactions. Superposition of the fundamental mode, A_{00} and the third- and fourth-order doughnut mode, B_{031} and B_{042} are shown, resulting in circling optical vortices. The interferograms show the phase dislocations.

dynamics are governed not only by the photorefractive response time, but also by the cavity's symmetry settings.

2. Interfamily Mode Beatings

Figure 2 shows clearly that cavity-length detunings exist that lead to a coexistence between the fundamental and the third- or fourth-order family. For a cylindrical symmetry the modes interact in the form of circling optical vortices.[16] Figure 12 shows three and four circling vortices observed as the beatings between the fundamental and third- and fourth-order family, respectively. Theoretically, circling vortices are obtained by the superposition of the fundamental mode and the doughnut mode, giving a number of vortices corresponding to the mode order of the doughnut. However, circling vortices are obtained even though the cavity symmetry is insufficient to sustain doughnut modes. Instead, they arise because of interactions between the fundamental mode and a superposition of the higher-order modes.

The direction of rotation depends on the charge of the doughnut vortices. A positive charge leads to a clockwise rotation. Rotation is seen to be opposite in the case of the third- and fourth-order mode interaction. The circling frequency is 33 mHz for the third-order and 50 mHz for the fourth-order interaction, which is determined by the frequency difference with respect to the fundamental mode. This indicates that the third-order modes are located closer to the fundamental mode in frequency space than are the fourth-order modes in agreement with Fig. 2.

One of the most interesting observations is that the circling vortex dynamics, occurring between the fundamental mode and the third- and fourth-order modes, are on the same time scale as the dynamics between modes belonging to the same family. This is remarkable because the frequency separation between adjacent transverse modes of the same family is in the order of hundreds of kilohertz[3] whereas different families are separated by tens of megahertz. A possible explanation is a much larger frequency pulling experienced by the higher-order modes relative to the fundamental mode. The frequency pulling increases with mode order, as a result of an increased linewidth caused by larger diffraction losses in the intracavity aperture. This reduces the mutual frequency separation between the fundamental mode and the third- and fourth-order mode family, respectively, giving beat frequencies of tens of megahertz.

4.   CAVITY SYMMETRY REGIONS

The previous sections reveal static and dynamic modes belonging to different mode bases and, thus, different degrees of cavity symmetry. Four symmetry regions of different mode properties are observed:

Rectangular cavity symmetry leading to stationary Cartesian (Gauss–Hermite) modes. These modes suggest a considerable amount of astigmatism between the two perpendicular axes. This leads to a large frequency separation between the perpendicular Cartesian modes of the same family. In this case $\Delta\nu_m \gg \Delta\nu_{crit}$, where $\Delta\nu_m$ is the frequency separation between the cavity modes and $\Delta\nu_{crit}$ is the critical frequency separation for phase locking between the modes. Purely linear modes (one order number equals zero) can also be achieved by inducing high losses in one direction. However, in that case the modes will be present in one direction only. When the cavity symmetry is increased, the cavity-mode separation decreases, but still $\Delta\nu_m > \Delta\nu_{crit}$. The system then reaches the border between rectangular and cylindrical symmetry. Here the circular modes exist as transients obtained by varying the cavity length, but they decay into stationary linear modes in seconds.

Partly cylindrical cavity symmetry leading to dynamical modes of Cartesian circular, and rotational symmetry. The almost cylindrical symmetry gives rise to beatings of the near degenerate intrafamily modes. This suggests that only a small asymmetry, leading to a small frequency separation, $\Delta\nu_m \approx \Delta\nu_{crit}$, is present. Only the A_{00} Laguerre mode is stationary; all higher-order modes appear as dynamic pattern sequences, some periodic. Beatings between different mode families are also observed in this region. An example is the circling vortices that are obtained by the superposition of the fundamental and the third- or fourth-order families as shown in Fig. 12.

Cylindrical cavity symmetry leading to stationary circular (Gauss–Laguerre) modes. This configuration requires a frequency separation smaller than the critical value, $\Delta\nu_m < \Delta\nu_{crit}$, which causes the perpendicular rectangular Gauss–Hermite modes to phase lock into Gauss–Laguerre stationary modes. Obtaining the Gauss–Laguerre flower modes demands cylindrical but, in general, not a full rotational symmetry. In our experiments stationary Laguerre modes are obtained only up to the second-order mode family. For higher-order modes the radial symmetry is slightly broken, probably owing to some minor optical defects in the system.

Rotational cavity symmetry leading to stationary Laguerre and doughnut modes of full rotational symmetry. This case corresponds to a frequency separation smaller than the critical value, $\Delta\nu_m < \Delta\nu_{crit}$, which results in frequency degeneracy between the Gauss–Laguerre flower modes A_{0l1} and A_{0l2}, causing them to phase lock into Gauss–doughnut stationary modes. This regime is not reached in these experiments.

The mode dynamics shown in this paper belong to the second symmetry region, partly cylindrical symmetry. This is a symmetry region that has not attracted much attention because it is in general desirable to be able to project all modes onto the same mode base. However our experiments show that this region includes much interesting spatial-mode dynamics on a time scale at least 1 order of magnitude different from that reported for a cylindrically symmetric photorefractive oscillator.[3]

5. CONCLUSION

We demonstrated experimentally the equivalence between different Gaussian mode bases in a photorefractive ring oscillator aligned to partly cylindrical symmetry. We have identified and characterized the symmetric properties that govern the modes and mode dynamics of the cavity. The PRO is shown to be capable of producing a nearly full set of transverse Gaussian modes up to the order of 4. Both linear, circular, and rotational symmetric modes are obtained. The choice of the mode base is strongly connected to the cavity symmetry, which is controlled mainly by the transverse position of the intracavity lens. For a partly broken cylindrical symmetry, modes belonging to different mode bases are seen to interact.

Dynamics in the form of periodic sequences and transformations from one mode to another are observed. The dynamics are theoretically explained by superpositions of modes taking their mutual phases into account. Both interactions between modes belonging to the same family and to different families are observed. Intrafamily interactions show transitions and periodic sequences between modes belonging to different mode bases, while interfamily interactions lead to circling vortex structures similar to the ones extensively studied in hydrodynamic systems. All of the observed dynamics are in the range of millihertz because of an extreme frequency pulling of the photorefractive two-beam coupling gain. Especially, the intrafamily modes with an empty cavity spacing of the order of hundreds of kilohertz interact with the same beat frequency as the modes of different families separated by tens of megahertz. A possible explanation is a larger degree of frequency pulling for higher-order modes that brings their oscillation frequency close to that of the fundamental mode when interacting. Finally, four different regimes of cavity symmetry leading to different modes and dynamic schemes have been identified. From rectangular, partly cylindrical, cylindrical, to rotational cavity symmetry, the symmetry is chosen by inducing or reducing the axial or rotational astigmatism. Here the region of partly cylindrical symmetry has been investigated for the first time to our knowledge.

*Present address, Cornelia Denz, Nichtlineare Optik und optische Informationsverarbeitung, Institut für Angewandte Physik, Westfälische Wilhelms-Universität, Corrensstr.   2-4,   48149 Münster/Westfalen,   e-mail: denz@uni-muenster.de.

REFERENCES

1. P. Pellat-Finet and J.-L. de la Tocnaye, "Optical generator of spheroidal wave functions using a BSO crystal," Opt. Commun. **55**, 305–310 (1985).
2. G. D'Alessandro, "Spatiotemporal dynamics of a unidirectional ring oscillator with photorefractive gain," Phys. Rev. A **46**, 2791–2802 (1992).
3. D. Hennequin, L. Dambly, D. Dangoisse, and P. Glorieux, "Basic transverse dynamics of a photorefractive oscillator," J. Opt. Soc. Am. B **11**, 676–684 (1994).
4. J. Malos, M. Vaupel, K. Staliunas, and C. O. Weiss, "Dynamical structures of a photorefractive oscillator," Phys. Rev. A **53**, 3559–3564 (1996).
5. B. M. Jost and B. E. A. Saleh, "Spatiotemporal dynamics of coupled-transverse-mode oscillations in unidirectional photorefractice ring resonators," Phys. Rev. A **51**, 1539–1548 (1995).
6. G. Balzer, C. Denz, O. Knaup, and T. Tschudi, "Circling vortices and pattern dynamics in a unidirectional photorefractive ring oscillator," Chaos, Solitons Fractals **10**, 725–730 (1999).
7. F. T. Arecchi, G. Giacomelli, P. L. Ramazza, and S. Residori, "Experimental evidence of chaotic itinerancy and spatiotemporal chaos in optics," Phys. Rev. Lett. **65**, 2531–2534 (1990).
8. M. Vaupel, K. Staliunas, and C. O. Weiss, "Hydrodynamic phenomena in laser physics: Modes with flow and vortices behind an obstacle in an optical channel," Phys. Rev. A **54**, 880–892 (1996).
9. P. Yeh, "Two-wave mixing in nonlinear media," Opt. Lett. **7**, 484–486 (1989).
10. H. Kogelnik and T. Li, "Laser beams and resonators," Appl. Opt. **5**, 1550–1566 (1966).
11. J. T. Verdeyen, *Laser Electronics* (Prentice-Hall, Upper Saddle River, New Jersey, 1981).
12. F. Encinas-Sanz, O. G. Calderón, R. Gutiérrez-Castrejón, and J. M. Guerra, "Measurement of the spatiotemporal dynamics of simple transverse patterns in a pulsed transversely excited atmospheric CO_2 laser," Phys. Rev. A **59**, 4764–4772 (1999).
13. M. Ciofini, A. Labate, R. Meucci, and P.-Y. Wang, "Experimental evidence of selection and stabilization of spatial patterns in a CO_2 laser by means of spatial perturbations," Opt. Commun. **154**, 307–312 (1998).
14. O. Svelto, ed. D. C. Hanna, translator and ed., *Principles of Lasers* 3rd ed. (Plenum Press, New York, 1989).
15. M. Brambilla, F. Battipede, L. A. Lugiato, V. Penna, F. Prati, C. Tamm, and C. O. Weiss, "Transverse laser patterns. I. Phase singulary crystals," Phys. Rev. A **43**, 5090–5113 (1991).
16. M. Vaupel, C. O. Weiss, "Circling optical vortices," Phys. Rev. A **51**, 4078–4085 (1995).